



# Formation of Interstellar C<sub>60</sub> from Silicon Carbide Circumstellar Grains

J. J. Bernal<sup>1</sup> , P. Haenecour<sup>2</sup>, J. Howe<sup>3</sup> , T. J. Zega<sup>2,4</sup> , S. Amari<sup>5</sup>, and L. M. Ziurys<sup>1,6,7</sup> 

<sup>1</sup>Department of Chemistry and Biochemistry, University of Arizona, Tucson, AZ 85721, USA; [lziurys@email.arizona.edu](mailto:lziurys@email.arizona.edu)

<sup>2</sup>Lunar and Planetary Laboratory, University of Arizona, 1629 E. University Boulevard, Tucson, AZ 85721, USA

<sup>3</sup>Department of Materials Science and Engineering, and Department of Chemical Engineering and Applied Chemistry, University of Toronto, Canada

<sup>4</sup>Department of Materials Science and Engineering, University of Arizona, USA

<sup>5</sup>Physics Department and McDonnell Center for the Space Sciences, Washington University in St. Louis, 1 Brookings Drive, St. Louis, MO 63130, USA

<sup>6</sup>Department of Astronomy, Steward Observatory, University of Arizona, 933 North Cherry Avenue, Tucson, AZ 85721, USA

<sup>7</sup>Arizona Radio Observatory, Steward Observatory, University of Arizona, 933 North Cherry Avenue, Tucson, AZ 85721, USA

Received 2019 May 25; revised 2019 August 30; accepted 2019 September 3; published 2019 October 1

## Abstract

We have conducted laboratory experiments with analog crystalline silicon carbide (SiC) grains using transmission electron microscopy (TEM) and electron energy-loss spectroscopy (EELS). The 3C polytype of SiC was used—the type commonly produced in the envelopes of asymptotic giant branch (AGB) stars. We rapidly heated small (~50 nm) synthetic SiC crystals under vacuum to ~1300 K and bombarded them with 150 keV Xe ions. TEM imaging and EELS spectroscopic mapping show that such heating and bombardment leaches silicon from the SiC surface, creating layered graphitic sheets. Surface defects in the crystals were found to distort the six-membered rings characteristic of graphite, creating hemispherical structures with diameters matching that of C<sub>60</sub>. Such nonplanar features require the formation of five-membered rings. We also identified a circumstellar grain, preserved inside the Murchison meteorite, that contains the remnant of an SiC core almost fully encased by graphite, contradicting long-standing thermodynamic predictions of material condensation. Our combined laboratory data suggest that C<sub>60</sub> can undergo facile formation from shock heating and ion bombardment of circumstellar SiC grains. Such heating/bombardment could occur in the protoplanetary nebula phase, accounting for the observation of C<sub>60</sub> in these objects, in planetary nebulae (PNs) and other interstellar sources receiving PN ejecta. The synthesis of C<sub>60</sub> in astronomical sources poses challenges, as the assembly of 60 pure carbon atoms in an H-rich environment is difficult. The formation of C<sub>60</sub> from the surface decomposition of SiC grains is a viable mechanism that could readily occur in the heterogeneous, hydrogen-dominated gas of evolved circumstellar shells.

*Key words:* astrochemistry – circumstellar matter – ISM: molecules – methods: laboratory: solid state – stars: AGB and post-AGB – stars: winds, outflows

## 1. Introduction

Buckminsterfullerene (C<sub>60</sub>) is a molecule with 60 carbon atoms assembled into five- and six-membered rings in a highly stable spherical configuration. The first identification of C<sub>60</sub> in an astrophysical environment was in the planetary nebula (PN) Tc 1 (Cami et al. 2010). The PN stage is the final evolutionary phase for most stars, following the asymptotic giant branch (AGB). By the PN phase, the stars have shed most of their original mass in outflowing winds, leaving behind a fading white dwarf. Subsequent detections of C<sub>60</sub> were made in the ISM (Sellgren et al. 2010), other galactic and extra-galactic PNs (García-Hernández et al. 2010), H-rich RCB stars (García-Hernández et al. 2011), proto-PNs (e.g., Zhang & Kwok 2011), YSOs (Roberts et al. 2012), and diffuse clouds (Berné et al. 2017). The C<sub>70</sub> fullerene was also identified in a few PNs (Cami et al. 2010; García-Hernández et al. 2011), and the C<sub>60</sub><sup>+</sup> cation has been suggested to account for a few of the diffuse interstellar bands, also referred to as the “DIBs” (Campbell et al. 2015). The origin of interstellar fullerenes, however, is uncertain. There is no facile mechanism that can readily link 60, sp<sup>2</sup>-hybridized carbon atoms together in environments that are rich in hydrogen and other elements under typical astrophysical conditions (Zhang & Kwok 2011). It therefore was originally proposed that C<sub>60</sub> formed only in H-deficient regions where polycyclic aromatic hydrocarbons (PAHs) and other hydrogen-containing molecules are not observed (Cami et al. 2010, 2011). Subsequent observations, however, have

shown that C<sub>60</sub> is prevalent in hydrogen-rich environments (including PN Tc 1; García-Hernández et al. 2010, 2011), further compounding the difficulty in explaining its formation; indeed, thus far C<sub>60</sub> has not been detected in any H-poor space environment.

In the terrestrial laboratory, C<sub>60</sub> is readily created in the high-collision environment of a supersonic jet expansion by laser ablation of pure graphite in the presence of helium, as was originally discovered by Kroto et al. (1985). It was later found that the species could also be produced in an arc discharge using graphite electrodes (Hare et al. 1991). Other synthesis methods, including those involving hydrogen, were not as successful in creating fullerenes. The addition of hydrogen, for example, to the gas expansion in a laser ablation source preferentially created PAHs as opposed to C<sub>60</sub> (De Vries et al. 1993). Using a 3:2 mixture of He and H<sub>2</sub> in the expansion was found to generate fullerene soot, but only at extremely high temperatures exceeding 4000 K (Jäger et al. 2009). Laser ablation of hydrogenated amorphous carbon (HAC) thin films was found to lead to fullerenes; however, smaller molecules containing ~40 C atoms are the dominant products in this process, not C<sub>60</sub> (Scott et al. 1997). Also, Carpentier et al. (2012) found disordered, “fullerene-like structures” in soot particles emulating HACs, while Duley & Hu (2012) suggested the presence of “protofullerenes” in Raman spectra of HAC analogs, but neither experimental study claimed evidence of C<sub>60</sub> in their data. Laboratory work by Tielens and collaborators

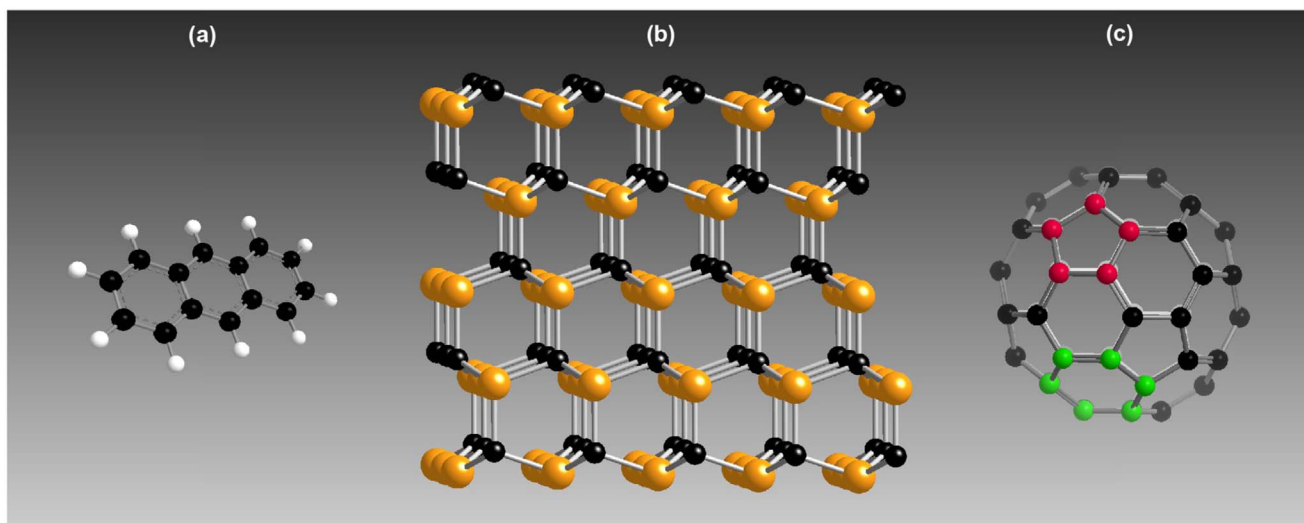


**Figure 1.** Relevant carbon structures. (a) A polycyclic aromatic hydrocarbon (PAH) molecule (anthracene). (b) The cubic (3C) polytype of silicon carbide, with Si atoms indicated in copper. (c) C<sub>60</sub> showing five-membered (red) and six-membered rings (green).

(e.g., Berné & Tielens 2012; Zhen et al. 2014; Zhang et al. 2019) suggests that PAHs may be a route to C<sub>60</sub>.

In an effort to further explore synthetic routes to interstellar/circumstellar C<sub>60</sub>, we have conducted experimental studies of the thermal decomposition of silicon carbide (SiC) grains using in situ transmission electron microscopy (TEM). Our experiments show that the heating and irradiation of the 3C polytype of SiC creates outer layers of graphene sheets and hemispherical carbon nanobuds. Here we present our measurements and analysis, and discuss their astronomical implications for C<sub>60</sub>.

## 2. Experimental

Studies of circumstellar “presolar” grains extracted from meteorites have shown that SiC is a common material, but has different crystalline structures, or polytypes. The 3C structure accounts for  $\sim 80\%$  of the SiC grain population (Daulton et al. 2002), and thus was chosen for the experiments. See Figure 1 for the chemical structure of SiC and related compounds.

A 3C-SiC sample (99% purity; U.S. Research Nanomaterials) was obtained with particle size of 45 to 65 nm—comparable to bona fide circumstellar grains (Jura 1994). Two types of samples were used: (1) pure “dry” SiC particles and (2) a slurry of SiC particles and methanol. These samples were deposited onto supporting SiN films (Norcada) for in situ heating and analysis, e.g., Thompson et al. (2017). The films consist of a microelectromechanical systems (MEMS) platform to provide uniform heating. The methanol slurry, as opposed to a dry sample, produces a uniform distribution of many particles over the film. However, there is potential contamination of the sample by methanol. On the other hand, clumping can occur in the dry sample during drop casting, resulting in a nonuniform particle distribution on the film, making TEM measurements difficult. Nonetheless, we were successful in getting particles dry cast onto the SiN film. Both types of samples, which were studied in separate experiments, gave equivalent results.

The MEMS support films were loaded into a Hitachi “Blaze” heating holder and loaded into the Hitachi H9000 TEM located in the intermediate voltage electron microscope tandem (IVEM) facility at Argonne National Laboratory (<https://www.ne.anl.gov/ivem/>). The holder allows for rapid heating

of the samples up to  $\sim 1300$  K. The IVEM is a dual-ion beam facility providing several different types of ions for irradiation (e.g., He, Xe, and Kr) over a range of energies (5 keV to 500 keV). High-resolution imaging is conducted in situ with the TEM as the samples are heated and/or irradiated.

The sample was heated at  $5^\circ\text{C min}^{-1}$  to  $1000^\circ\text{C}$ , or  $\sim 1300$  K under a vacuum of  $10^{-6}$  Pa ( $\sim 10^{-11}$  atm—very close to actual circumstellar conditions; Ziurys 2006). Once that temperature was reached, irradiation was started at 150 keV with Xe ions. The combined rapid heating and irradiation were done to mimic shock heating in circumstellar shells. Xe and other noble gases have been found embedded in SiC grains, believed to be caused by high speed post-AGB winds with energies  $\sim 100$ – $800$  keV (Verchovsky et al. 2004; Heck et al. 2009). The “wet” sample was irradiated for 2 hr with up to 15 displacements per atom (dpa), while the sample was held at  $1000^\circ\text{C}$ . The drycast sample was irradiated for only 1 hr with a weaker dosage of 3 dpa. All other experimental parameters were the same for both samples.

After in situ heating and irradiation, the samples were analyzed using the University of Arizona 200 keV Hitachi HF5000 aberration-corrected scanning transmission electron microscope (S/TEM). The HF5000 has a spatial resolution of 0.23 nm in TEM mode (parallel illumination), and 0.078 nm in scanning mode (converged beam). It is equipped with a CCD camera for imaging in TEM mode, bright-field, dark-field, secondary-electron detectors for STEM imaging, and energy-dispersive X-ray (EDS) and electron energy-loss (EELS) spectrometers for chemical analysis. The HF5000 is further equipped with alignments at 200 keV and 60 keV. The EELS analyses were conducted first at the C, K absorption edge at 60 keV, after which high-resolution imaging was performed at 200 keV. We used 60 keV for the EELS analysis, which is below the threshold energy for C displacement, in order to avoid any potential damage to the sample during imaging and analysis (Williams & Carter 2009). The C, K EELS edge occurs because of the excitation of core-shell  $1s$  electrons to empty  $2p$  states.

In addition to the studies of analog SiC grains, a circumstellar grain (KFC1b2-gr1), thought to be composed entirely of graphite, was extracted from the Murchison

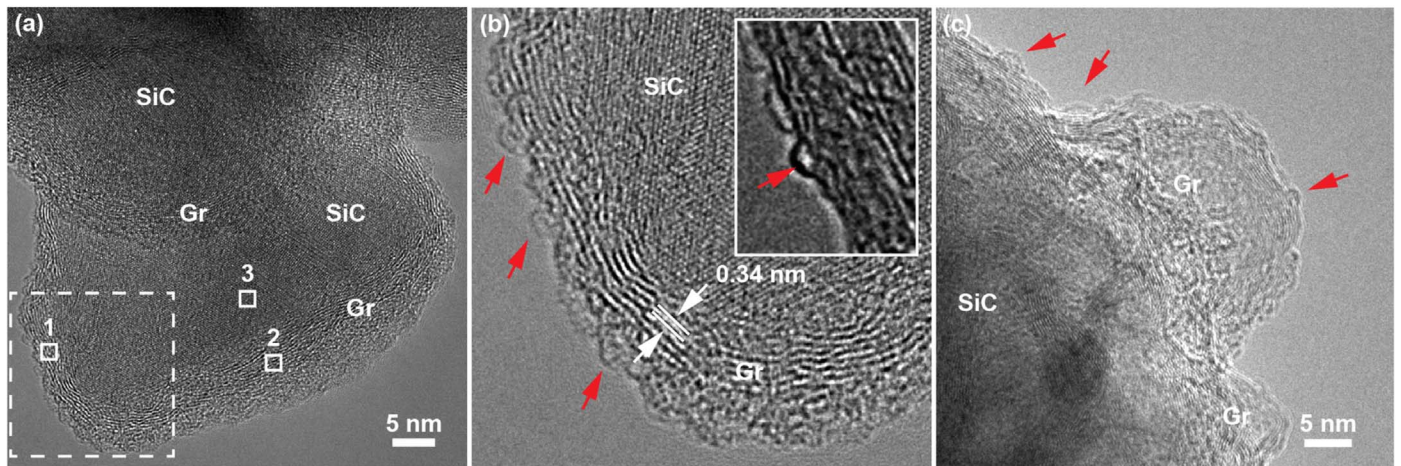


**Figure 2.** TEM images of model SiC grains, shock-heated under vacuum. (a) High-resolution image of two overlapping grains showing the SiC core, surrounded by surface layers of graphite (labeled Gr). Small boxes (1–3) indicate areas where EELS spectra were observed (Figure 3). (b) High-resolution image of grain section from Figure 2(a) (dashed box), showing hemispherical and near spherical structures (red arrows) on the surface, suggestive of  $C_{60}$ . The inset shows a TEM image of a  $C_{60}$  molecule on a nanotube (Duan et al. 2017). Our structures and that in the inset show similar diameters of  $\sim 0.7$  nm. White lines show the 0.34 nm interplanar (002) d-spacing characteristic of graphite; this scale applies to the entire image and inset. (c) High-resolution image of another heated SiC grain, also showing graphite layers and hemispherical carbon structures.

meteorite. A cross-section of the grain was prepared following focused-ion-beam (FIB) techniques (Zega et al. 2007) using the dual-beam Thermo Scientific Helios NanoLab 660 FIB-SEM at the University of Arizona. High-resolution STEM imaging, EDS mapping and EELS measurements of the grain cross-section were then carried out using a Hitachi SU9000 SEM/STEM with a 30 kV accelerating voltage. The carbon and oxygen isotopic compositions of the grain were additionally measured using nanoscale secondary ion mass spectrometry (NanoSIMS) at Washington University. We acquired ion images of C and O isotopes ( $^{12}\text{C}$ ,  $^{13}\text{C}$ ,  $^{16}\text{O}$ ,  $^{17}\text{O}$ , and  $^{18}\text{O}$ ) of the grain cross-section using a focused  $\text{Cs}^+$  primary beam of  $\sim 0.3$  pA that was rastered over a  $7.5 \times 7.5 \mu\text{m}^2$  surface ( $256 \times 256$  pixels $^2$ ) with a dwell time of 1 millisecond pixel $^{-1}$ .

### 3. Results

During heating/irradiation of the analog grains, the SiC surface crystal structure was significantly altered. The outer layers of the grains were transformed into graphitic sheets as silicon was leached from the lattice, as shown by the high-resolution TEM image in Figure 2(a). The image shows two grains that contain parallel sets of lattice fringes, visible as striated alternating bright and dark layers that conform to the grain surface. These fringes correspond to the (002) atomic planes with a periodic spacing of 0.34 nm and are due to graphite formation (labeled “Gr”) on the surface of the SiC. The image shows that the interior of the grains also contains parallel sets of lattice fringes, corresponding to the bulk SiC lattice, but they terminate at the edge of the particles where the layered graphite fringes occur. Note that the intrinsic structure of the 3C lattice (Figure 1) naturally leads to six-carbon ring formation as the silicon atoms are removed (Mishra et al. 2016). Defects in the crystal surface, on the other hand, promote the creation of hemispherical structures, as shown in Figures 2(b) and (c). Figure 2(b) displays a portion of the grain in Figure 2(a) outlined by the dashed box, magnified by a factor of  $\sim 2.5$ . On the outer layers of the grain, hemispherical and quasi-spherical structures occur, as indicated by red arrows. Such nonplanar features require the presence of five-membered

rings (Figure 1) with seven-membered rings at the graphene boundary (Watanabe et al. 2001). The diameter of the ring-like structures is  $\sim 0.7$  nm—very similar to that of  $C_{60}$ , as shown in the inset to the right in Figure 2(b). The inset displays a TEM image of a  $C_{60}$  molecule attached to a nanotube (Duan et al. 2017). Another heated SiC grain from our sample is presented in Figure 2(c). More hemispherical, nanobud-like structures are visible at the grain surface (see the red arrows).

The chemical content of the grain in Figure 2(a) was further investigated with EELS, as shown in Figure 3. This technique measures the energy lost by an electron beam as a result of inelastic scattering with atoms in the sample. Spectra extracted from three positions on the grain sample, shown by small solid boxes labeled 1, 2, and 3 in Figure 2(a), are presented on the left (a) in Figure 3. Positions 1 and 2 sample the graphitic layers on the grain edge, while Position 3 resides on the SiC region. The spectra from Positions 1 and 2 show two main peaks at 285.6–287.6 eV and at 289.6–294.9 eV. The lower-energy peak is well-known to arise from  $1s$  to  $\pi^*$  (antibonding) transitions, characteristic of the delocalized, aromatic carbon as found in graphite; the higher energy line is due to  $1s$  to  $\sigma^*$  (antibonding) transitions that trace single, aliphatic bonds to carbon, present in both graphite and SiC. The position 3 spectrum shows no evidence of aromatic bonding and therefore no graphite, arising exclusively from SiC. Positions 1 and 2 contain both aromatic and aliphatic carbon—clear evidence of graphite—which corroborates the high-resolution imaging shown in Figure 2. Reconstructed images of the two spectral features are displayed in Figure 3, right, (b)–(e). Panel (b) shows the gray-scale as-acquired spectrum image, while (c) features the aromatic  $\pi^*$  peak (red), which clearly is concentrated at the graphitic surface layers. The aliphatic  $\sigma^*$  peak (blue) in panel (d) is widespread, tracing both the unaltered SiC core and the graphitic material. The composite image, shown in panel (e), further highlights the differences in the spatial distribution of the C bonding.

The analysis of the circumstellar “graphite” grain KFC1b2-gr1 provides additional evidence for the formation of pure carbon structures from SiC. First, the isotopic composition of the grain showed high  $^{12}\text{C}$  enrichment

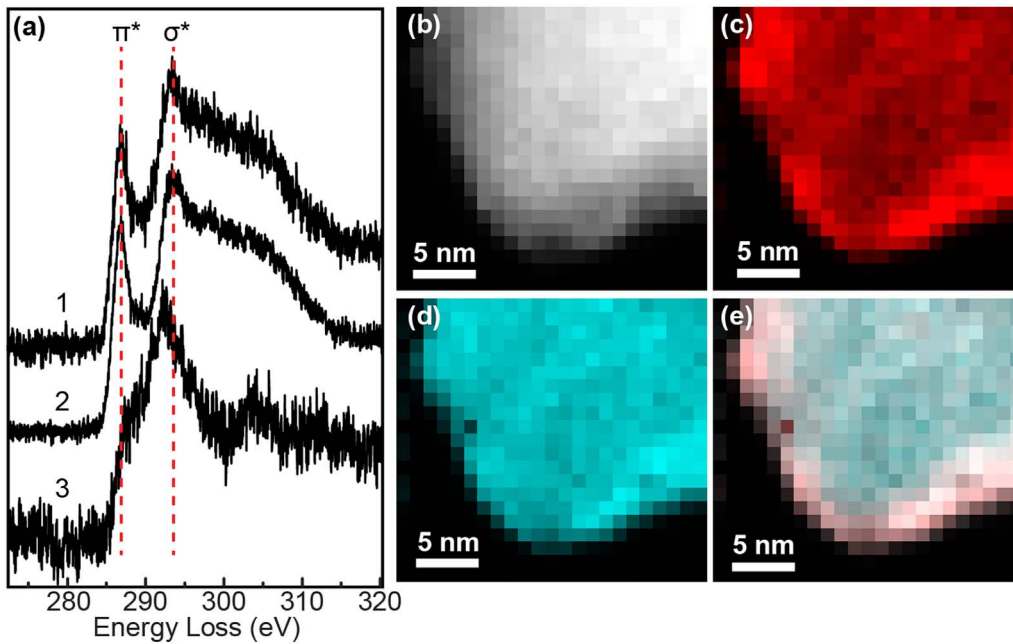


**Figure 3.** EELS data of the model SiC grain shown in Figure 2. (a) EELS spectra from the boxed regions of the grain indicated in Figure 2(a). Spectral peaks observed at Positions 1 and 2 indicate the presence  $\pi^*$  (aromatic) and  $\sigma^*$  (aliphatic) peaks, identifying the material as graphite, whereas Position 3 only shows a  $\sigma^*$  peak, consistent with SiC. (b) Reference spectrum image of the grain shown in Figure 2(a). (c) Extracted image of  $\pi^*$  distribution (red), revealing location of graphite. (d) Extracted image of  $\sigma^*$  distribution (light blue), tracing both graphite and SiC. (e) Composite image revealing SiC core (light blue) and graphite shell (red).

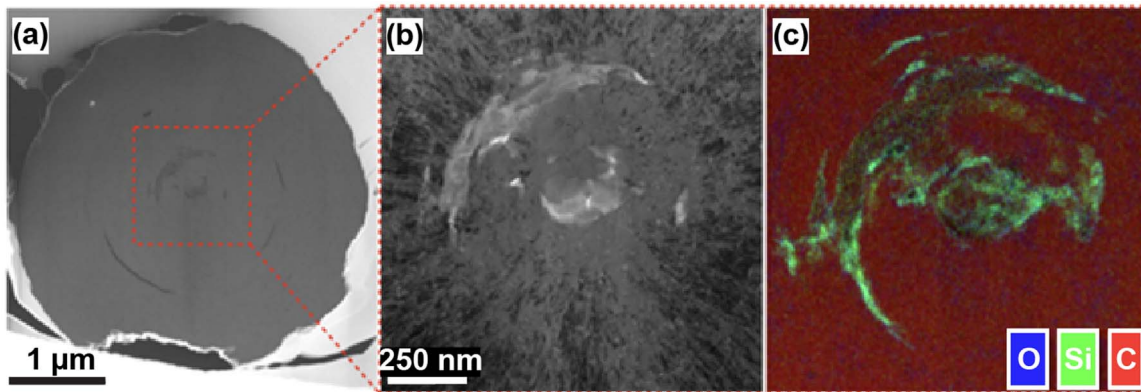


**Figure 4.** Scanning transmission electron microscopy (STEM) data of presolar graphite grain KFC1b2-gr1. (a) STEM bright-field image. (b) STEM bright-field image of the central grain core, indicated by the red box in (a). (c) Composite elemental EDS maps (oxygen = blue, silicon = green, and carbon = red) of the grain core. The elemental distribution shows the presence of the remnant of an SiC core surrounded by graphitic carbon.

( $^{12}\text{C}/^{13}\text{C} = 1546 \pm 248$ ), compared with the solar system value ( $^{12}\text{C}/^{13}\text{C} = 89$ ), consistent with an origin in the envelope of a low-mass C-rich AGB star. Second, the imaged cross-section of the grain displayed an unexpected morphology; see Figure 4. Figure 4(a) shows the full grain cross-section. Figure 4(b) presents a magnified version of the visibly irregular grain core, indicated by the red box in Figure 4(a). EDS chemical images of this core, presented in Figure 4(c), clearly shows that the disrupted center of the grain is mostly silicon, arising from SiC, entirely surrounded by graphitic carbon. This microstructure is consistent with our experimental analog grain results.

Observations of PN IC 418 also provide possible evidence for the proposed origin of  $\text{C}_{60}$ . In this source, the 17.4 mm feature of  $\text{C}_{60}$  and the 11.75 mm feature attributed to SiC dust grains were measured across the nebula (Díaz-Luis et al. 2018). Note that the SiC feature varies from that seen in AGB stars,

indicating some processing by the PN phase (García-Hernández 2012), and possibly acquiring a graphitic coating, consistent with our experiments. Two different flux calibration methods were used for the IC 418 images: synthetic photometry and the standard stars method. Although the emission of  $\text{C}_{60}$  is quite weak and at the detection limits, it shows some spatial correlation with the ring-like distribution of SiC, when the standard stars method was used, especially in the northeast outer regions, as shown in Figure 5 (also Figure 7 of Díaz-Luis et al.). However, when the synthetic photometry method was employed, the fullerene emission does not follow that of SiC, and is mainly located at the northeast, extending from the inner (even near the central star) to the outer regions of the nebula (Figure 6 of Díaz-Luis et al.). On the other hand, as noted by Díaz-Luis et al., by slightly changing the subtraction factor of the synthetic photometry calibration, the ring-like structure of  $\text{C}_{60}$  is recovered. These current results are

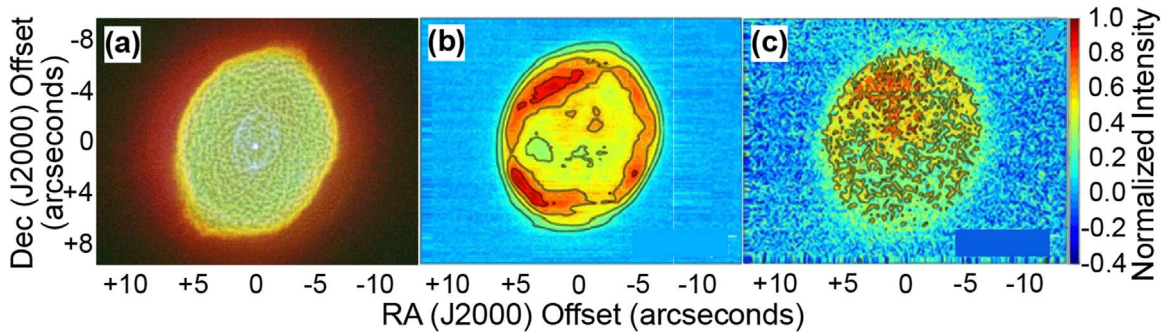


**Figure 5.** Observations toward PN IC 418. (a) *HST* image composite of [OIII] (blue), [H $\alpha$ ] (green), and [NII] (red) emission (Ramos-Larios et al. 2012), (b) IR images of the 9–13  $\mu\text{m}$  carrier (attributed here to SiC) and (c) residual C<sub>60</sub> emission, based on data from Díaz-Luis et al. (2018). The SiC and C<sub>60</sub> images were created by subtraction of continuum emission from 11.75  $\mu\text{m}$  filter data and continuum 20.5  $\mu\text{m}$  emission from 17.65  $\mu\text{m}$  filter observations, respectively. The standard stars flux calibration method was used for the SiC and C<sub>60</sub> images (see the text). Intensity scale is on the right ordinate. The distributions of SiC and C<sub>60</sub> show some similarity, which could be consistent with C<sub>60</sub> forming from SiC, but other interpretations are still possible (see, e.g., Díaz-Luis et al. 2018) until higher sensitivity mid-IR images would be obtained.

thus inconclusive, and further observations of C<sub>60</sub> in IC 418 are needed for a definitive interpretation.

## 4. Discussion

### 4.1. Comparison with Previous Studies

Similar experiments involving synthetic SiC polytypes, aimed at industrial semiconductor production, were previously performed (e.g., Mishra et al. 2016), which corroborate our findings. For example, smooth wafers of the hexagonal 6H polytype of SiC, which has a similar crystal structure to the 3C polytype, were heated under vacuum (Van Bommel et al. 1975; Mishra et al. 2016). Silicon was found to evaporate from the outer layers at temperatures as low as 800°C, creating a monolayer of graphene from the collapse of carbon atoms of three successive SiC layers (see Figure 1). When bombarded with hot H atoms, experiments suggest that the graphene sheets may lead to PAHs (Merino et al. 2014). Furthermore, carbon nanotubes with fullerene-like endcaps can be grown perpendicular to the crystal plane from 3C SiC, when heated with a YAG laser to 1800°C (Kusunoki et al. 1997). Both single and double-walled nanotubes with caps also formed on heating 3C-SiC to 1360°C (Watanabe et al. 2001). In this case, a diameter of  $\sim 0.8$  nm was found for several of the single-walled nanotubes, similar to that of C<sub>60</sub>. The cap formation was attributed to the lifting of graphite sheets, generating the necessary five-membered rings. Nanocap formation was additionally found to take place in the presence of H<sub>2</sub> (Ueda et al. 2010). Molecular dynamics simulations have shown that hemispherical carbon structures (or “buckybowls”) easily close to form stable fullerenes (Lebedeva et al. 2012). Our data suggest that C<sub>60</sub> is forming in our samples.

Previous TEM studies found other graphite presolar grains with SiC cores (Croat et al. 2010). Such grains, including KFC1b2-gr1, defy equilibrium thermodynamic models that predict a graphite core surrounded by SiC. Typical SiC condensation occurs after graphite formation except under extreme high-pressure conditions ( $>10^{-4}$  atm), characteristic of supernovae explosions but not AGB outflows (e.g., Croat et al. 2010).

Our experimental results on model SiC grains account for the unexpected grain structure and their AGB origin. Thermodynamic conditions favor SiC condensation, followed by shock heating to form reduced carbon nanostructures. Observations have also shown that SiC grains, although prominent in AGB

envelopes, are not observed in the ISM, leading to some speculation that they acquire a carbon mantle and therefore become invisible in the infrared (Dorschner & Henning 1995).

### 4.2. Implications for Interstellar/Circumstellar C<sub>60</sub>

SiC grains are readily created in circumstellar shells of AGB stars (Kwok 1993). As these stars leave the AGB and become PNs, more violent mass loss occurs (Kwok 1993; Sevenster & Chapman 2001; Van de Steene & van Hoof 2003). As a consequence, higher-velocity outflows are generated that can produce shocks in the slower AGB wind carrying the SiC dust, instantaneously raising the temperature of the material in excess of 1000 K (Sevenster & Chapman 2001; Van de Steene & van Hoof 2003). They also can accelerate ions that impact and implant into the grain surfaces (e.g., Heck et al. 2009). Such shock heating and bombardment can disrupt the SiC grains (Van de Steene & van Hoof 2003), in analogy to our experimental conditions, producing graphite and reduced carbon nanostructures which can lead to C<sub>60</sub>, and even possibly PAHs (Merino et al. 2014). Therefore, interstellar fullerenes can be created from shocked, circumstellar SiC grains, without the need for dehydrogenation, carbon atom elimination, and any dimensional constraint on the precursor material, such as PAH size (Berné et al. 2015). Indeed, shocks are thought to be associated with C<sub>60</sub> formation in post-AGB stars (Roberts et al. 2012). Photoprocessing of the grains may also aid in creating C<sub>60</sub> (see Kusunoki et al. 1997).

A simple calculation for the PN Tc 1 shows that there is sufficient SiC grain abundance to account for the C<sub>60</sub> in this source (Cami et al. 2010; García-Hernández et al. 2012). Estimates by García-Hernández et al. (2012) provide a gas phase carbon mass of  $3.00 \times 10^{-4}$  solar masses in Tc 1. Assuming a mass ratio of solid state to gas phase carbon of one, based on depletions in diffuse gas (Savage & Sembach 1996), then  $6.00 \times 10^{-4}$  solar masses of C exists in Tc 1. With a presumed C/Si ratio of 10, the silicon mass present is  $6.00 \times 10^{-5}$  solar masses. If 50% of available Si is present in SiC grains, the mass of condensed Si is  $3.00 \times 10^{-5}$  solar masses. Based on the stoichiometry of SiC, then  $\sim 1.50 \times 10^{-5}$  solar masses of C present in these grains. If 1% of this carbon is converted to C<sub>60</sub> by shock processing,  $1.50 \times 10^{-7}$  solar masses of C<sub>60</sub> is produced. This mass exceeds the  $5.8 \times 10^{-8}$  solar masses of C<sub>60</sub> estimated by Cami et al. (2010) in Tc 1. If

silicon or carbon undergoes further depletion, even more  $C_{60}$  will be produced.

$C_{60}$  is known to have an extreme longevity in high-energy photon environments (Cataldo et al. 2009). Its high stability enables it to survive into the PN stage, and then be ejected, along with other molecular material, into the diffuse ISM, where it is also observed in ionized form (Berné et al. 2017; Schmidt et al. 2018). Our findings also suggest that other carbon nanostructures such as nanotubes and “buckybowls” may be created in significant quantities by SiC grain shock heating and are transported into the ISM. Such structures may be a major sink of interstellar carbon and possible carriers of the DIBs.

The authors thank Prof. Krishna Muralidharan for insights into carbon nanostructures. This work was supported by NSF grants AST-1515568, 1531243, AST-1907910, NASA grants NNX15AD94G, NNX15AJ22G, NNX16A31G, NNX12AL47G, 80NSSC19K0509, NIH grant R25GM062584, DOE Contract DE-AC07-051D14517, and the Sloan Foundation Baseline Scholars Program.

### ORCID iDs

J. J. Bernal  <https://orcid.org/0000-0001-6176-0773>  
 J. Howe  <https://orcid.org/0000-0001-9319-3988>  
 T. J. Zega  <https://orcid.org/0000-0002-9549-022X>  
 L. M. Ziurys  <https://orcid.org/0000-0002-1805-3886>

### References

- Amari, S., Zinner, E., & Gallino, R. R. 2014, *GeCoA*, **133**, 479  
 Berné, O., Cox, N. L. J., Mulas, G., & Joblin, C. 2017, *A&A*, **605**, L1  
 Berné, O., Montillaud, J., & Joblin, C. 2015, *A&A*, **557**, A133  
 Berné, O., & Tielens, A. G. G. M. 2012, *PNAS*, **109**, 401  
 Cami, J., Bernard-Salas, J., Peeters, E., & Malek, S. E. 2010, *Sci.*, **329**, 1180  
 Cami, J., Bernard-Salas, J., Peeters, E., & Malek, S. E. 2011, in IAU Symp. 280, *The Molecular Universe*, ed. J. Cernicharo & R. Bachiller (Cambridge: Cambridge Univ. Press), **216**  
 Campbell, E. K., Holz, M., Gerlich, D., & Maier, J. P. 2015, *Natur*, **523**, 322  
 Carpentier, Y., Féraud, G., Dartois, E., et al. 2012, *A&A*, **548**, A40  
 Cataldo, F., Strazzulla, G., & Iglesias-Groth, S. 2009, *MNRAS*, **394**, 615  
 Croat, T. K., Stadermann, F. J., & Bernatowicz, T. J. 2010, *AJ*, **139**, 2159  
 Daulton, T. L., Bernatowicz, T. J., Lewis, R. S., et al. 2002, *Sci.*, **296**, 1852  
 De Vries, M. S., Reihs, K., Wendt, H. R., et al. 1993, *GeCoA*, **57**, 933  
 Díaz-Luis, J. J., García-Hernández, D. A., Manchado, A., et al. 2018, *AJ*, **155**, 105  
 Dorschner, J., & Henning, T. 1995, *A&ARv*, **6**, 271  
 Duan, S., Liu, X., Wang, Y., et al. 2017, *RSC Advances*, **7**, 21124  
 Duley, W. W., & Hu, A. 2012, *ApJL*, **745**, L11  
 García-Hernández, D. A. 2012, in IAU Symp. 283, *Planetary Nebulae: An Eye to the Future*, ed. A. Manchado, L. Stanghellini, & Schoenberner (Cambridge: Cambridge Univ. Press), **148**  
 García-Hernández, D. A., Iglesias-Groth, S., Acosta-Pulido, J. A., et al. 2011, *ApJL*, **737**, L30  
 García-Hernández, D. A., Manchado, A., García-Lario, P., et al. 2010, *ApJL*, **724**, L39  
 García-Hernández, D. A., Rao, N. K., & Lambert, D. L. 2011, *ApJ*, **729**, 126  
 García-Hernández, D. A., Villaver, E., García-Lario, P., et al. 2012, *ApJ*, **760**, 107  
 Hare, J. P., Kroto, H. W., & Taylor, R. 1991, *CPL*, **177**, 394  
 Heck, P. R., Amari, S., Hoppe, P., et al. 2009, *ApJ*, **701**, 1415  
 Jäger, C., Huisken, F., Mutschke, H., Llamas Jansa, I., & Henning, T. 2009, *ApJ*, **696**, 706  
 Jura, M. 1994, *ApJ*, **434**, 713  
 Kroto, H. W., Heath, J. R., O'Brien, S. C., Curl, R. F., & Smalley, R. E. 1985, *Natur*, **318**, 162  
 Kusunoki, M., Rokkaku, M., & Suzuki, T. 1997, *ApPhL*, **71**, 2620  
 Kwok, S. 1993, *ARA&A*, **31**, 63  
 Lebedeva, I. V., Knizhnik, A. A., Popov, A. M., & Potapkin, B. V. 2012, *J. Phys. Chem. C*, **116**, 6572  
 Merino, P., Švec, M., Martínez, J. I., et al. 2014, *NatCo*, **5**, 3054  
 Mishra, N., Boeckl, J., Motta, N., & Iacopi, F. 2016, *PSSAR*, **213**, 2277  
 Ramos-Larios, G., Vázquez, R., Guerrero, M. A., et al. 2012, *MNRAS*, **423**, 3753  
 Roberts, K. R. G., Smith, K. T., & Sarre, P. J. 2012, *MNRAS*, **421**, 3277  
 Savage, B. D., & Sembach, K. R. 1996, *ARA&A*, **34**, 279  
 Schmidt, D. R., Zack, L. N., & Ziurys, L. M. 2018, *ApJL*, **864**, L31  
 Scott, A., Duley, W. W., & Pinho, G. P. 1997, *ApJL*, **489**, L193  
 Sellgren, K., Werner, M. W., Ingalls, J. G., et al. 2010, *ApJL*, **722**, L54  
 Sevenster, M. N., & Chapman, J. M. 2001, *ApJL*, **546**, L119  
 Thompson, M. S., Zega, T. J., & Howe, J. Y. 2017, *M&PS*, **52**, 413  
 Ueda, K., Iijima, Y., Maruyama, T., & Naritsuka, S. 2010, *Journal of Nanoscience and Nanotechnology*, **10**, 4054  
 Van Bommel, A. J., Crombeen, J. E., & Van Tooren, A. 1975, *SurSc*, **48**, 463  
 Van de Steene, G. C., & van Hoof, P. A. M. 2003, *A&A*, **406**, 773  
 Verchovsky, A. B., Wright, I. P., & Pillinger, C. T. 2004, *ApJ*, **607**, 611  
 Watanabe, H., Hisada, Y., Mukainakano, S., & Tanaka, N. 2001, *JMic*, **203**, 40  
 Williams, D. B., & Carter, C. B. 2009, *Transmission Electron Microscopy: A Textbook for Materials Science* (2nd ed.; New York: Springer Science)  
 Zega, T. J., Nittler, L. R., Busemann, H., Hoppe, P., & Stroud, R. M. 2007, *M&PS*, **42**, 1373  
 Zhang, W., Yubing, S., Zhen, J., et al. 2019, *ApJ*, **872**, 38  
 Zhang, Y., & Kwok, S. 2011, *ApJ*, **730**, 126  
 Zhen, J., Castellanos, P., Paardekooper, D. M., Linnartz, H., & Tielens, A. G. G. M. 2014, *ApJL*, **797**, L30  
 Ziurys, L. M. 2006, *PNAS*, **103**, 12274